

MAGNETOROTATIONAL INSTABILITY CAN SUSTAIN TURBULENCE FROM TANGLED SMALL-SCALE FIELDS

PALLAVI BHAT¹, FATIMA EBRAHIMI¹,

Department of Astrophysical Sciences and Princeton Plasma Physics Laboratory, Princeton University, Princeton, NJ 08543, USA

ERIC G. BLACKMAN²

Department of Physics and Astronomy, University of Rochester, Rochester, NY 14618, USA

AND

KANDASWAMY SUBRAMANIAN³

Inter University Centre for Astronomy and Astrophysics, Post Bag 4, Pune University Campus, Ganeshkhind, Pune 411 007, India

(Dated: September 23, 2016)

Draft version September 23, 2016

ABSTRACT

The initial conditions used in previous magnetorotational instability (MRI) simulations always consisted of a significant large or system-scale component, even if random. However it is of both conceptual and practical interest to assess whether the MRI can sustain when the initial field is turbulent, correlated on scales much smaller than the given system. More generally, we also study what minimum conditions the initial random small-scale field must have for the MRI to sustain the turbulence. The ubiquitous presence of turbulent or random flows in the high magnetic Reynolds number astrophysical plasmas in galaxies or stars for example, leads to a small-scale dynamo (SSD). This can generate random magnetic fields in the plasma that eventually enters an accretion disk. To simulate this scenario, we take the random field generated by the SSD as the input initial condition to a shearing box simulation that has uniform shear and rotation but with the forcing turned off. We find that the system becomes unstable to the MRI which then sustains the turbulence. The saturated stresses, large scale fields and power spectra in such simulations match the standard MRI simulation with an initial vertical large scale mode with zero net flux. For Gaussian random field initial conditions, the MRI does not grow. For MRI to grow, we determine that there is both a minimum field strength and minimum field coherence, which can be met naturally by an initial field configuration generated by the SSD, the most common form of magnetic field generation in the universe.

Subject headings: magnetic fields—dynamo—turbulence—accretion, accretion disks

1. INTRODUCTION

Magnetic fields are ubiquitous in turbulent astrophysical plasmas. While the mechanism of origin of large scale ordered magnetic fields in these systems is a subtle business, more generic and less controversial is the amplification of total magnetic energy by the fluctuation or small-scale dynamo (SSD). Here, turbulence in a conducting plasma, with even a modest magnetic Reynolds number (R_m), leads to exponential growth on the shortest eddy turn over time scales, which is usually much smaller than the age of the astrophysical system. The SSD is likely to be important for the early generation of magnetic fields in stars and galaxies/inter-stellar medium (ISM) (Sur et al. 2010; Gent et al. 2013; Bhat & Subramanian 2013). Such SSD generated fields would then be present in the plasma from stars or the ISM that source accretion disks.

In previous studies of the magneto-rotational instability (MRI) in shearing box models of accretion disks, the initial condition is typically an ordered *non-stochastic* field with net flux or zero-net flux. Following linear stability analysis, this kind of initial condition is the most natural to compare with minimalist analytic theory, but in reality one expects a more random field without necessarily much of a large scale field. The question then arises as to whether and what kind of disorder and incoherence in the initial field can still lead to MRI and field growth.

In the case of initial vertical fields of zero flux or net flux

field, the MRI modes grow large scale radial and azimuthal fields in the early linear growth phase (Bhat et al. 2016a; Ebrahimi & Blackman 2016) on orbital times scales eventually saturating nonlinearly to generate turbulence. It has been a long-standing topic of investigation to understand what determines the amplitude of the fields and stresses on MRI saturation, because this is thought to constrain the rate of angular momentum transport in accretion disks. The saturation amplitude of the stresses is not a constant across simulations but, for fixed resolution and box dimensions, depends on whether the initial field is of zero-net flux type or there is a uniform background field (Hawley et al. 1995; Fromang & Papaloizou 2007; Guan et al. 2009; Shi et al. 2016).

Here we investigate whether random fields (without a significant large scale component) can seed the MRI, and whether the MRI sustains. Previous work using initially random fields (Hawley et al. 1996) had adopted a flat 1-D magnetic spectrum, and also with mostly large scale modes having $1 < k(L/2\pi) < 4$ and the field being 0 outside that interval. Such an initial field has a significant large scale component, (with the box scale field comparable to smaller scale fields), unlike the initial conditions we adopt below. In particular, we show that using small-scale fields from a small-scale dynamo (SSD) as an initial condition, subsequent shear and rotation act to trigger MRI and as a result, sustains the turbulent fields even after the SSD forcing is turned off. We also discuss that the MRI fails to sustain when Gaussian random fields are instead used as an initial condition.

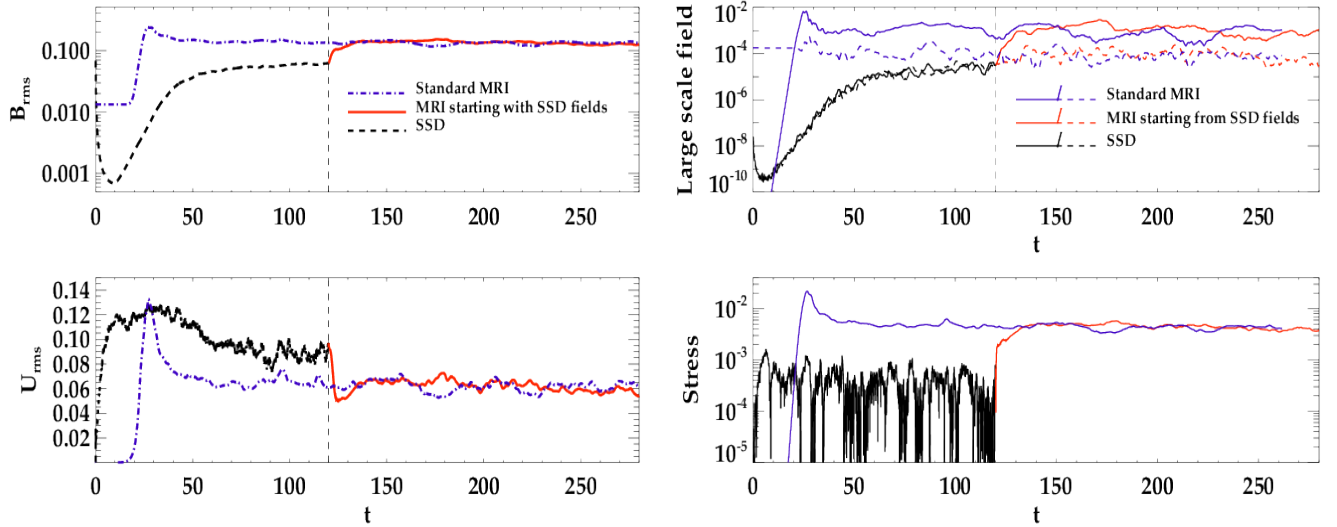


FIG. 1.— Evolution of B_{rms} and U_{rms} is shown in upper and lower left panels respectively for Run SSD, Run A and Run STD. Evolution of energy in large scale magnetic fields and sum of Maxwell and Reynold stresses is shown in upper and lower right panels respectively for Run SSD, Run A and Run STD. The solid curves refer to x - y averaged fields while the dashed curves refer to y - z averaged fields.

In section 2, we compare the sustained MRI turbulence with SSD initial condition against the case with zero net flux initial condition, with respect to the standard MRI signatures. Section 3 discusses the role of coherence in initial random magnetic fields for MRI to grow. The nature of MRI starting with SSD generated fields is investigated by spectral analysis in Section 4. We conclude in Section 5.

2. SUSTAINED MRI TURBULENCE WITH SSD INITIAL CONDITION

We perform shearing box simulations in a periodic box of $1 : 1 : 1$ aspect ratio using the PENCIL CODE¹. Most simulations are of the resolution of 256^3 grid points. The simulations are performed in two stages. First, to obtain the initial condition, we run a simulation of the SSD, without shear or rotation, with an imposed isotropic stochastic forcing in the momentum equation. Second, the velocity and magnetic fields from this small-scale dynamo simulation (either from the kinematic or saturated stage), are introduced into a shearing box simulation as initial condition, with uniform shear $U_y = Sx$ (where S is the shearing rate) and rotation. The rotation is obtained by adding the Coriolis force term in the momentum equation, $2(\Omega \times U)$, where $\Omega = \Omega_0 \hat{z}$. In all of our runs, $S = -1.5$ and $\Omega_0 = 1$. Note that the stochastic forcing term used to obtain the SSD saturated state is subsequently turned off when the shearing box simulation begins with the SSD generated field as its initial condition.

In Fig. 1, we show the evolution of root mean square magnetic and velocity fields over time, for three runs (i) The SSD simulation run to saturation which is used to set the initial condition, called Run SSD (ii) the shearing box MRI simulation with initial fields from this SSD simulation, referred to as Run A, starting at $t \sim 120$; and (iii) a standard MRI run starting with zero net flux of vertical large scale mode, Run STD. The magnetic Reynolds number is defined as $R_m = U_{\text{rms}} L / \eta$, where L is the size of the box and η is the microscopic resistivity and $R_m = 12000$ for Run SSD and in Run STD and Run A, the resulting R_m is 6000. The Prandtl number is $\text{Pr}_M = \nu / \eta$ and $\text{Pr}_M = 10$ for all the three runs. It can be seen that for Run A (shown in solid red lines), initial

saturated SSD fields do not decay but grow and sustain due to MRI. The B_{rms} grows by a factor of ~ 2 to a value ~ 0.13 and U_{rms} decays by a factor of ~ 2 , saturating at a value of ~ 0.06 . Interestingly the saturation levels of both B_{rms} and U_{rms} match with those from Run STD. Fig. 1 also shows that the U_{rms} decays to a value which is smaller than the B_{rms} , thus going from a kinetically dominated system (SSD saturation phase) to a magnetically dominated system as would be the case for MRI turbulence.

We show the Reynolds and Maxwell stresses $\langle U_x U_y \rangle$ and $\langle B_x B_y \rangle$ for Run A compared to Run STD in the lower right panel of Fig. 1. The amplitude of the sum of the stresses in Run A is ~ 0.005 , which is the same as in Run STD. On the other hand, the stresses in Run SSD are very noisy and orders of magnitude below those of Run A. A distinctive increase at $t \sim 120$ is seen, indicating the presence of MRI instability. We find that the Maxwell to Reynolds stress ratio in Run A is about 6.9, which matches well with the ratio ~ 6.7 estimated from the standard MRI simulation, Run STD.

In the upper right panel of Fig. 1, we also show the evolution of planar averaged large scale fields. The solid lines refer to x - y averaged fields and the dashed lines show the y - z averaged fields. The growth in the large scale field in Run SSD is due to the low wavenumber tail of the magnetic power (peaked at large k) that results because the SSD eigenfunction grows self-similarly across all scales (Bhat & Subramanian 2013; Subramanian & Brandenburg 2014; Bhat et al. 2016b). However the saturation level is rather small at 10^{-5} . In the standard MRI simulation, the large scale dynamo amplifies low wavenumber fields to a much higher amplitude $\sim 10^{-3}$ (Bhat et al. 2016a), and this also obtains in Run A. In fact, from Fig. 1 top right panel, we see that again the amplitude of energy in large scale fields from Run A matches with Run STD.

3. IMPORTANCE OF COHERENCE SCALES

3.1. SSD vs. Gaussian random Initial Conditions

Unlike the case of the SSD initial conditions discussed in the previous section, we find that for a Gaussian random field of even a large initial RMS field strength $B_{\text{rms}} \sim 0.1$, the field and velocity fluctuations decay in the shearing box run.

¹ <https://github.com/pencil-code> (Brandenburg 2003)

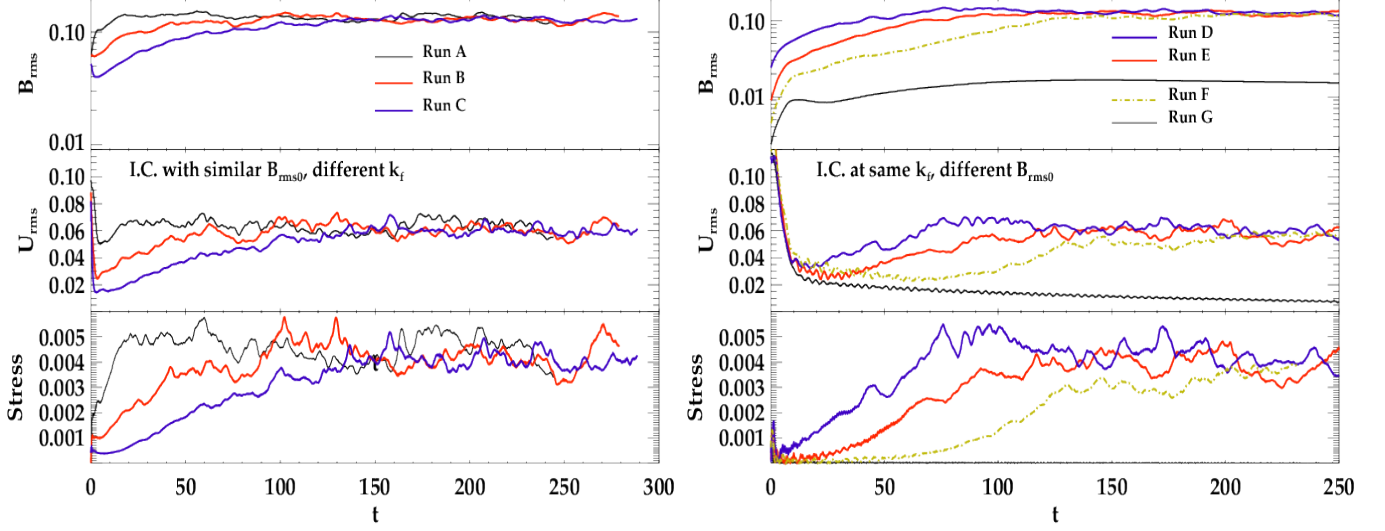


FIG. 2.— Evolution of B_{rms} and U_{rms} and stresses is shown in upper, middle and lower panels respectively for varying k_f in initial SSD fields in the left set and for varying $B_{\text{rms}0}$ in the right set. In the left set: the black, red and blue curves correspond to Run A, Run B and Run C where initial fields have $k_f = 1.5$, 5 and 10 respectively with similar $B_{\text{rms}0}$ around ~ 0.06 . In the right set: the blue, red, dashed green and black curves correspond to Run D, Run E, Run F and Run G where initial fields have $k_f = 1.5$, but decreasing $B_{\text{rms}0}$.

| Run | k_f | $B_{\text{rms}0}$ | $U_{\text{rms}0}$ | $\gamma_{B_{\text{rms}}}$ |
|-----|-------|-------------------|-------------------|---------------------------|
| A | 1.5 | 0.06 | 0.095 | 0.0274 |
| B | 5 | 0.06 | 0.09 | 0.0088 |
| C | 10 | 0.05 | 0.08 | 0.0053 |
| D | 1.5 | 0.02 | 0.12 | 0.0158 |
| E | 1.5 | 0.008 | 0.12 | 0.0153 |
| F | 1.5 | 0.004 | 0.12 | 0.0146 |
| G | 1.5 | 0.002 | 0.12 | - |

TABLE 1

SUMMARY OF ALL RUNS: FOR EACH RUN, THE FORCING SCALE k_f OF THE SSD RUN FROM WHICH THE INITIAL CONDITION IS TAKEN IS SPECIFIED. ALSO SHOWN ARE THE INITIAL MAGNETIC AND VELOCITY FIELD STRENGTHS, $B_{\text{rms}0}$ AND $U_{\text{rms}0}$ AND THE GROWTH RATE OF B_{rms} GIVEN BY $\gamma_{B_{\text{rms}}}$. ALL RUNS HERE ARE OF 256^3 RESOLUTION.

This Gaussian random field was obtained by setting the vector potential to be normally distributed, uncorrelated random numbers in all meshpoints for all three components, which results in a spherical shell averaged magnetic power spectrum, \mathcal{E}_M , that increases with wave number k as $\mathcal{E}_M \sim k^4$. Note on the other hand, such Gaussian random field used as the initial condition in the Run SSD, does indeed lead to field growth.

Why is the MRI triggered when the initial fields come from a SSD but not from Gaussian random fields? To answer this, the role of the magnetic integral scale (or the typical coherence scale) of the initial SSD fields on MRI is important to assess. In the SSD simulations, the forcing term in the momentum equation drives vortical motions localised around a wavenumber k_f , changing direction and phase at every time step (more details are given in Haugen et al. (2004)). Thus the the turbulent outer scale of the velocity field is set at $k = k_f$. The growing magnetic fields in the SSD, peak near the resistive scales in the kinematic phase; but by saturation, the power shifts to larger scales closer to k_f (Bhat & Subramanian 2013). Therefore, we must investigate the effect of increasing k_f during the SSD phase and how this influences subsequent sustenance of MRI turbulence once the stochastic forcing is turned off.

3.2. Sensitivity of MRI to the k_f of the initial saturated SSD fields

Fig. 2 shows the time evolution of B_{rms} , U_{rms} and stresses in MRI simulations with initial SSD fields whose forcing wavenumbers were $k_f = 1.5$, 5 and 10, indicated by black, blue and red lines respectively. The one with $k_f = 1.5$ is the same as Run A shown in Fig. 1. The runs with $k_f = 5$ and 10 are referred to as Run B and Run C respectively. The time axis is normalised to start from $t=0$ (so the Run A shown to start at $t \sim 120$ in Fig. 1, starts from $t = 0$ here). The plots show that increasing k_f decreases the growth rate and thus increases the time to reach saturation. This implies that the MRI modes which are triggered must be of larger wavenumber k for initial fields of larger k_f . One can perhaps understand this as follows: For an initially uniform vertical field B_0 , MRI unstable modes have a maximum growth rate for a wavenumber $k = k_{\text{max}} \propto \Omega/B_0$. One may roughly adopt a similar estimate for random fields, with now B_0 a measure of a suitably defined local coherent component of the field. For larger k_f , the magnetic power from the SSD is also peaked at a larger k , and for the same RMS value of the field, the B_0 would be smaller or k_{max} would be larger. These larger MRI unstable k modes are more affected by damping than lower k modes and thus incur smaller growth rates. The above interpretations also explain why an initial seed field of Gaussian random noise doesn't trigger MRI; namely that the coherence scale would be close to the grid resolution scale. Note however that a Gaussian random noise seed field does lead to SSD action in forced turbulence, as mentioned earlier.

3.3. Sensitivity of MRI to the strength of initial kinematic SSD fields

While the saturated SSD fields seem to be sufficiently coherent to trigger the MRI for a broad range of k_f we can also ask whether SSD fields from just the kinematic regime are locally coherent enough to trigger MRI? We investigate this here using fields from the kinematic regime of SSD as initial condition for MRI.

The right panel of Fig. 2 shows the time evolution of total B_{rms} , U_{rms} and stresses in MRI simulations with SSD gen-

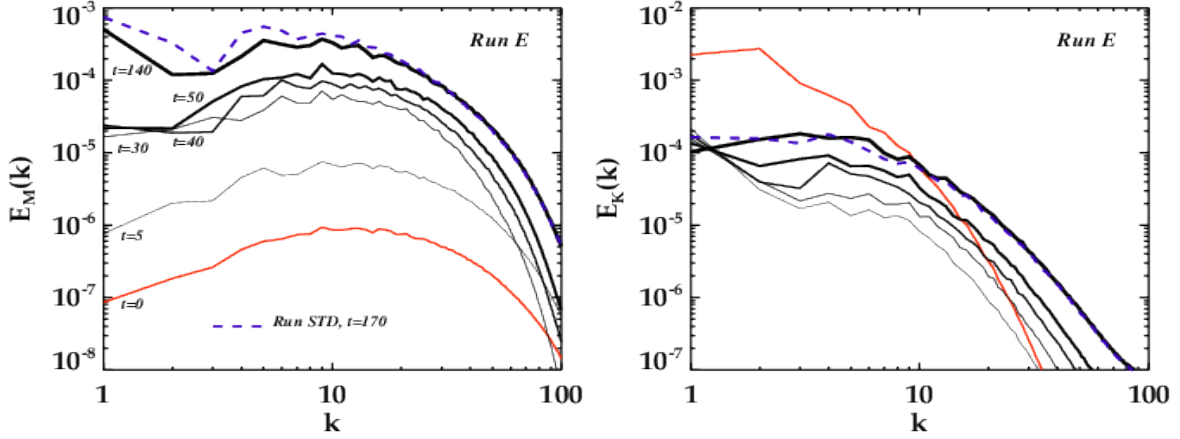


FIG. 3.— Evolution of magnetic power spectrum is shown in the left panel at times $t = 5, 30, 40, 50$ and 140 in solid black line of increasing thickness. Similarly kinetic power spectrum is shown in the right panel at times $t = 30, 40, 50, 60$ and 140 in solid black line of increasing thickness. These are shown for Run E. The red curves are the initial spectra. And the dashed green curves correspond to the spectra from Run STD in saturation.

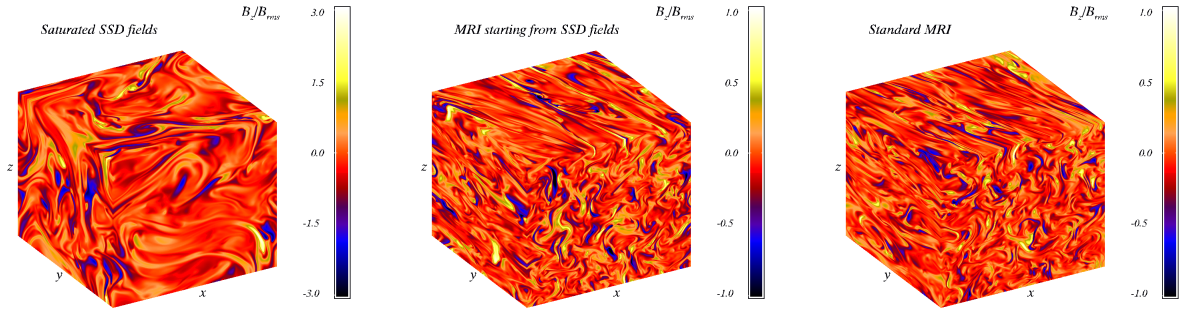


FIG. 4.— The vertical component of the magnetic fields are plotted for Run SSD, Run A and Run STD at a higher resolution of 512^3 in left, middle and right panels, from the saturated regimes.

erated fields from the kinematic regime, of different initial field strengths $B_{\text{rms}0}$, but the same $k_f = 1.5$. The different curves are for $B_{\text{rms}0} \sim 0.02, 0.008, 0.004, 0.002$, shown in solid blue, solid red, dash-dotted green and solid black respectively; also referred as Run D, Run E, Run F and Run G. We find that MRI is triggered for initial SSD fields even from its kinematic regime. Again, here we find a trend of decreasing growth rate with decreasing $B_{\text{rms}0}$. Note that as we decrease the initial field, we also decrease the effective B_0 , and so increase the wavenumber of the fastest growing mode, where damping effects can slow down the growth.

Note that the magnetic field growth happens in two regimes, as seen from the evolution curves of B_{rms} and U_{rms} in the right panels of Fig. 2. At first, even as U_{rms} decays due to rapid turbulent cascade of the velocity, B_{rms} actually grows rapidly due to enhanced random shearing from these velocity flows. By “enhanced random shearing”, we mean that even though the velocity field is decaying, the flow is still turbulent and there is a temporary SSD action enhanced by the uniform shear. But this gets subsequently overtaken by MRI action. Thereafter both B_{rms} and U_{rms} grow together due to MRI at the same rate up unto saturation. In the bottom-most curve in upper right panel of Fig. 2 in black, there is an initial increase of the magnetic field due to the random shearing, which however is not enough to trigger modes which are sufficiently large scale to compete with diffusion. Thus MRI modes do not grow in this particular run with $B_{\text{rms}0} \sim 0.002$. And while the velocity field (U_{rms}) decays further, the magnetic

field, after the initial rapid growth due to random shearing, turns to saturate but continues to grow at a smaller rate due to the linear shearing action. However it eventually decays as it gets stretched out to resistive scales. We therefore show that the strength of total initial turbulent fields also has a critical role in triggering the MRI here.

Additionally, we considered the case in which SSD fields were allowed to decay (by removing the external forcing). Then such decayed (not fully) fields were used as initial condition for MRI. We again found that the MRI grows and saturates to the same amplitude as the other MRI growth cases. This is conceptually motivated by the possible circumstance whereby a disk forms from the collapse of a turbulent cloud or object whose forcing may not survive the transition. We have summarised the initial condition parameters for the different runs studied, in the Table 1. The growth rate of the B_{rms} calculated for each run is an average quantity given by $\gamma_{B_{\text{rms}}} = (\int_0^T dt d(\ln B_{\text{rms}})/dt)/T$, where T is the time taken to reach saturation.

4. SPECTRAL ANALYSIS OF MRI GROWTH

To understand how the power spectrum of the turbulent initial field evolves once the MRI takes over and whether there are any modal signatures akin to standard MRI linear phase, we study the initial SSD fields to MRI spectral evolution. Fig. 3 shows the evolution of magnetic and kinetic power spectra in Run E (corresponding to the solid red curves in right panel of Fig. 2) in the left and right panels respectively.

The magnetic power spectrum, \mathcal{E}_M , first grows self-similarly from $t = 0$ to $t = 5$, due to enhanced random shearing action (similar to how the SSD spectrum grows c.f. Schekochihin et al. (2004)). Then during $t = 30$ to $t = 50$, the growth is due to MRI (when both B_{rms} and U_{rms} grow together). Here the MRI modes smaller than $k \sim 2-3$ do not grow much even if they correspond to maximally growing modes because they transfer all of their energy to larger wavenumbers. This indicates why the larger wavenumbers all grow by the same amount. A similar picture is seen for the kinetic spectra, \mathcal{E}_K , with little growth at lower wavenumbers ($k \sim 1-3$), but higher wavenumbers growing in unison. Note that between $t = 50$ to 140, the small k modes become more and more prominent. Finally, the thickest solid black curves in both panels from the saturated regime are compared with the dashed curve at a similar time from the standard MRI run and they match well.

Note the peak at $k = 1$, which also indicates presence of large scale fields (besides planar averaging). We find that the peak at $k = 1$ appears and disappears periodically, consistent with temporal cycles in the large scale dynamo associated with planar averaged fields. Unlike runs in elongated shearing boxes, along with the peak at $k = 1$, there is a second peak around $k = 4-5$. Further investigation of these features is beyond the scope of the present paper.

Lastly, we show the vertical component of magnetic fields from Run SSD, Run A and Run STD with a higher resolution of 512^3 in Fig. 4. For Run SSD, most of the box is orange indicating weaker small-scale fields. The scattered appearance of yellow or blue regions (both indicating higher magnitude fields) is due to the intermittency of the SSD. For Run A and Run STD, there are longer more coherent structures, particularly in the azimuthal direction, indicating the presence of large scale fields. Also there are stronger small-scale fields as well, indicating higher contributions to Maxwell stresses compared to Run SSD. Note the characteristic vertical loop structures (an MRI signature) in the $x-z$ plane in both Run A and Run STD. Thus Run A and Run STD compare well indicating that such simulations (with zero net flux) are indepen-

dent of the respective initial conditions.

5. CONCLUSIONS

In this letter, we have shown via direct numerical simulations that the MRI can sustain MHD turbulence even when seeded with an initially random small-scale but not too incoherent field. When the initial field is supplied by an SSD, MRI growth results but when the initial field is a Gaussian random field, the MRI fails to grow. The SSD is a natural initial condition as it is likely to be common in sufficiently conducting plasmas as in stars or the galactic ISM that feed accretion flows.

We find that the saturated state of the magnetic and velocity fields in our simulations starting with an SSD initial condition, are almost indistinguishable from that of the more commonly studied case of initial vertical fields of zero net flux. In particular the saturated amplitudes of the total magnetic and velocity fields (magnetic field being dominant), the accretion stresses, ratio of Maxwell to Reynolds stress, and the magnetic and kinetic power spectra are all very similar for the two aforementioned initial conditions.

Overall, our results have enabled us to identify following minimal requirements on initial conditions required to trigger the MRI: 1) the turbulent initial fields must be sufficiently coherent, and 2) the initial fields must be sufficiently strong. As the coherence scale of initial fields is decreased or the strength lowered, smaller scale MRI modes are triggered which grow at slower rates due to the influence of diffusion/damping. If the initial coherence scales or field strengths are too small, the MRI is quenched from growth by diffusion. Studying MRI with such a random/turbulent initial condition is expected to further the progress in understanding MRI saturation and also the large scale dynamo therein.

We thank Jim Stone and Greg Hammett for thoughtful questions and discussions and Luca Comisso and Manasvi Lingam for some useful suggestions. PB and FE acknowledge grant support from DOE, de-sc0012467. EB acknowledges support from grants HST-AR-13916.002, and NSF AST1515648. The computing resources were provided by Princeton Institute of Computational Science (PICSciE).

REFERENCES

- Bhat, P., Ebrahimi, F., & Blackman, E. G. 2016a, MNRAS, 462, 818
 Bhat, P., & Subramanian, K. 2013, MNRAS, 429, 2469
 Bhat, P., Subramanian, K., & Brandenburg, A. 2016b, MNRAS, 461, 240
 Brandenburg, A. 2003, in *Advances in Nonlinear Dynamos*, ed. A. Ferriz-Mas & M. Núñez (Taylor & Francis, London and New York), 269–344
 Ebrahimi, F., & Blackman, E. G. 2016, MNRAS, 459, 1422
 Fromang, S., & Papaloizou, J. 2007, *Astronomy & Astrophysics*, 476, 1113
 Gent, F. A., Shukurov, A., Sarson, G. R., Fletcher, A., & Mantere, M. J. 2013, MNRAS, 430, L40
 Guan, X., Gammie, C. F., Simon, J. B., & Johnson, B. M. 2009, ApJ, 694, 1010
 Haugen, N. E., Brandenburg, A., & Dobler, W. 2004, PRE, 70, 016308
 Hawley, J. F., Gammie, C. F., & Balbus, S. A. 1995, ApJ, 440, 742
 —. 1996, ApJ, 464, 690
 Schekochihin, A. A., Cowley, S. C., Taylor, S. F., Maron, J. L., & McWilliams, J. C. 2004, ApJ, 612, 276
 Shi, J.-M., Stone, J. M., & Huang, C. X. 2016, MNRAS, 456, 2273
 Subramanian, K., & Brandenburg, A. 2014, MNRAS, 445, 2930
 Sur, S., Schleicher, D. R. G., Banerjee, R., Federrath, C., & Klessen, R. S. 2010, ApJ, 721, L134